

**Fig. 5.** Cortical migration defects in *Brn-1*<sup>-/-</sup> brain. (A and B) BrdU-labeled (A) and immunostaining of Tst-1<sup>+</sup> (B) neurons in midlateral cortical sections of wild-type and *Brn-1*<sup>-/-</sup> brains. (C and D) Indirect immunofluorescent colocalization of Brn-1 and Tst-1 (C) or reelin (D) in wild-type P0 midlateral coronal cortex. (E) Reelin-specific in situ hybridization signal in high and low magnifications of P0 wild-type and *Brn-1*<sup>-/-</sup> coronal cortex; arrows in low-magnification view of *Brn-1*<sup>-/-</sup> indicate increased reelin expression in basal ganglia relative to wild type. (F) Immunoperoxidase detection of mDab1 expression in midlateral coronal wild-type P1 *Brn-1*<sup>-/-</sup> cortex. Scale bars: (B), 40  $\mu$ m; (C), 50  $\mu$ m; (A), 100  $\mu$ m; (F), 125  $\mu$ m; and (E), 250  $\mu$ m.

observed superficial location of Tst-1 neurons in *Brn-1*<sup>-/-</sup> cortex and the reduced migration of layer II/III neurons might reflect influences of a Brn-1-dependent, cell-autonomous mechanism analogous to that described in the *Brn-1*<sup>-/-</sup>/*Brn-2*<sup>-/-</sup> cortex.

Unexpectedly, the expression of reelin in a subpopulation of cortical plate neurons that colocalize with Brn-1 at P0 (Fig. 5D), and reportedly with markers of inhibitory interneurons in postnatal brain (20), was absent in the *Brn-1*<sup>-/-</sup> cortex, whereas reelin expression was unaffected in Cajal-Retzius neurons and even increased in basal ganglia areas (Fig. 5E), where Brn-1 expression is also normally observed (8, 9, 12). Potential roles, if any, for these Brn-1<sup>+</sup>, reelin-secreting neurons in cortical development remain to be defined, but we reproducibly found a detectable increase in mDab1-specific immunohistochemical staining in the *Brn-1*<sup>-/-</sup> in the neocortical plate (Fig. 5F), consistent with the observation that the intracellular levels of mDab1 protein increase in the absence of reelin signaling (14).

Together, these studies link Brn-1 and Brn-2 to the regulation of radial migration of layers II-V, at least in part, through regulation of the p39/p35 regulatory components of CDK5, resulting in cortical inversion in *Brn-1*<sup>-/-</sup>/*Brn-2*<sup>-/-</sup> double gene-deleted mice and disorganized cortical lamination in *Brn-1*<sup>-/-</sup> mice, where radial migration of layers II/III is delayed.

**References and Notes**

1. P. Rakic, *Science* **183**, 425 (1974).
2. S. A. Anderson, D. D. Eisenstat, L. Shi, J. L. Rubenstein, *Science* **278**, 474 (1997).
3. D. S. Rice, T. Curran, *Annu. Rev. Neurosci.* **24**, 1005 (2001).

4. J. Herz, *Neuron* **29**, 571 (2001).
5. J. A. Cooper, B. W. Howell, *Cell* **97**, 671 (1999).
6. D. S. Smith, P. L. Greer, L. H. Tsai, *Cell Growth Differ.* **12**, 277 (2001).
7. J. Ko et al., *J. Neurosci.* **21**, 6758 (2001).
8. X. He et al., *Nature* **340**, 35 (1989).
9. G. Alvarez-Bolado, M. G. Rosenfeld, L. W. Swanson, *J. Comp. Neurol.* **355**, 237 (1995).
10. M. D. Schonemann et al., *Genes Dev.* **9**, 3122 (1995).
11. See supplementary Web material (26) for Web figs. 1 to 5.
12. R. J. McEvilly, M. G. Rosenfeld, data not shown.
13. See supplementary Web material (26) for immunodetection, in situ hybridization, BrdU cell labeling, and TUNEL methodologies.
14. D. S. Rice et al., *Development* **125**, 3719 (1998).
15. T. Takahashi, T. Goto, S. Miyama, R. S. Nowakowski, V. S. Caviness Jr., *J. Neurosci.* **19**, 10357 (1999).
16. T. Allen, C. G. Lobe, *Cell. Mol. Biol.* **45**, 687 (1999).
17. D. Acampora, P. Barone, A. Simeone, *Cereb. Cortex* **9**, 533 (1999).
18. C. Zhou et al., *Neuron* **24**, 847 (1999).
19. P. A. Leighton et al., *Nature* **410**, 174 (2001).
20. S. Alcantara et al., *J. Neurosci.* **18**, 7779 (1998).
21. P. Li et al., *Genes Dev.* **7**, 2483 (1993).
22. H. Fujii, H. Hamada, *Neuron* **11**, 1197 (1993).
23. Y. Shang, X. Hu, J. DiRenzo, M. A. Lazar, M. Brown, *Cell* **103**, 843 (2000).
24. See supplementary Web material (26) for chromatin immunoprecipitation details.
25. R. J. McEvilly, M. G. Rosenfeld, in preparation.
26. Supplementary material is available on Science Online at [www.sciencemag.org/cgi/content/full/295/5559/1528/DC1](http://www.sciencemag.org/cgi/content/full/295/5559/1528/DC1).
27. The authors thank M. Becker-André for RORB cDNA, T. Curran and D. Rice for reelin and mDab1 in situ probes; A. Goffinet for reelin antisera; B. Howell for mDab1 antisera; J. Rubenstein for Dlx-2 cDNA; A. Wynshaw-Boris for reagents; A. Ryan for Brn-1/Brn-2 antisera; and L. Erkman, O. Hermanson, and K. Scully for critical reading and discussion. We thank E. Mears and P. Myer for figure preparation and H. Taylor and M. Frazer for animal husbandry. R.J.M. was a recipient of a National Alliance for Research on Schizophrenia and Depression young investigator award; M.G.R. is an Investigator with Howard Hughes Medical Institute. This research was supported by a grant from the National Institute of Neurological Disorders and Stroke.

15 October 2001; accepted 18 January 2002

## Functional MRI of Macaque Monkeys Performing a Cognitive Set-Shifting Task

Kiyoshi Nakahara,<sup>1</sup> Toshihiro Hayashi,<sup>1,2</sup> Seiki Konishi,<sup>1</sup> Yasushi Miyashita<sup>1,3\*</sup>

Functional brain organization of macaque monkeys and humans was directly compared by functional magnetic resonance imaging. Subjects of both species performed a modified Wisconsin Card Sorting Test that required behavioral flexibility in the form of cognitive set shifting. Equivalent visual stimuli and task sequence were used for the two species. We found transient activation related to cognitive set shifting in focal regions of prefrontal cortex in both monkeys and humans. These functional homologs were located in cytoarchitecturally equivalent regions in the posterior part of ventrolateral prefrontal cortex. This comparative imaging provides insights into the evolution of cognition in primates.

The prefrontal cortex (PFC) is evolutionarily most developed in primates and supports higher cognitive functions. Macaque mon-

keys have been widely used for investigating the PFC, mainly in anatomical, electrophysiological, and lesion studies (1–5), whereas

## REPORTS

the human PFC has been mainly investigated in neuroimaging and neuropsychological studies (6–10). We thus wanted to compare directly the functional organization of the PFC between the two species using a common physiological technique (11, 12). Recently, functional magnetic resonance imaging (fMRI) studies have been performed in both anesthetized and awake macaque monkeys (13–18). In the present study, we applied event-related fMRI to macaque monkeys and humans performing a modified version of the Wisconsin Card Sorting Test (WCST). The WCST (8) has been used to probe behavioral flexibility, i.e., the ability to shift from one response tendency (cognitive set) based on previous experiences, to another that is suitable for the current circumstances. Performance in this test is characteristically impaired by lesions of the PFC in both humans (8, 9) and monkeys (4, 5). In our modified WCST, equivalent task sequence and visual stimuli were used in subjects of the two species for the direct comparison (19, 20) (Fig. 1, A and B).

Two macaque monkeys (monkeys Y and Z) were trained to perform the modified WCST (21). To confirm that the monkeys behaved according to the rule of the task, behavioral data in fMRI sessions were assessed in three different ways. First, we assessed how efficiently the monkeys could complete each set shifting. For both monkeys, more than 80% of shifts were completed within three trials (monkey Y, 327 out of 395 shifts; monkey Z, 343 out of 394 shifts) (22). The mean number of trials required to complete a shift was  $2.3 \pm 1.9$  in monkey Y and  $1.7 \pm 1.6$  in monkey Z (mean  $\pm$  SD). Second, we assessed types of errors to analyze the monkeys' strategy after dimensional changes. Two types of errors are possible: perseverative errors and nonperseverative errors. Perseverative errors were the errors that resulted from continuing to make responses according to the previously relevant dimension. Nonperseverative errors were the errors that resulted from making responses that did not match in any dimension (Fig. 1A). If monkeys tend to make random selections (i.e., neglecting dimensions) expecting chance hits, the percentages of perseverative errors will approach 50%. Among errors at the time of dimensional changes, excluding inevitable errors immediately after dimensional changes, the perseverative errors accounted for  $83.4 \pm 4.9\%$  in monkey Y and

$86.4 \pm 5.8\%$  in monkey Z, significantly above 50% ( $P < 10^{-7}$ ; binomial test). Finally, once the monkeys completed each instance of set shifting and established a current cognitive set, they had to maintain it until the next dimensional change. We examined performance of trials between each completion of shifting and the next dimensional change. The mean correct response was  $93.8 \pm 2.7\%$  in monkey Y and  $92.3 \pm 2.0\%$  in monkey Z (chance level, 33.3%,  $P < 10^{-7}$ ; binomial test). These results confirmed that the monkeys' performances were proficient and that their behaviors were in good accordance with the rule of the WCST that requires both shifting and maintenance of cognitive set.

Functional images of the two monkeys were obtained by echo-planer imaging (EPI) with a voxel size of  $2 \times 2 \times 2.5$  mm (23). All of the images were spatially normalized to a template that we made from three-dimensional (3D) anatomical images of one monkey's whole brain (24). This procedure enabled us to perform a group analysis of the monkeys using SPM 99, and to introduce a stereotaxic coordinate arranged in bicommissural space in which the origin was placed at the anterior commissure (16). The EPI images overlapped faithfully with the corresponding reference images (23). The predicted hemodynamic responses to each dimensional change

were modeled based on the general linear model implemented in SPM 99 (Fig. 1C). Such an event-related modulation of the fMRI signals reflects brain activation that was locked to the time of occurrence of cognitive set shifting (25).

The group analysis revealed transient activation associated with set shifting in the monkeys' bilateral inferior prefrontal convexity (Fig. 2, A and B) (26). The peak of the activation was located in the rostral bank at the ventral end of the inferior ramus of the arcuate sulcus. FMRI signals from these activation foci were transiently increased (0.5 to 0.6%) time-locked to the set-shifting event (Fig. 2B). Transient activation was also found in the rostral bank of the left intraparietal sulcus, the bilateral posterior cingulate cortex, the precuneus, and the insula (26). To confirm the reproducibility of this activation across the monkeys, the data from each monkey were analyzed independently. Bilateral prefrontal activation foci were observed in the same cortical regions across the monkeys (Fig. 2C), and their coordinates showed overlap between the subjects (26). These results support intersubject reproducibility of activated regions in the PFC. We further performed another type of group analysis, a conjunction analysis that is suggested to be adequate to infer typical characteristics of a pop-

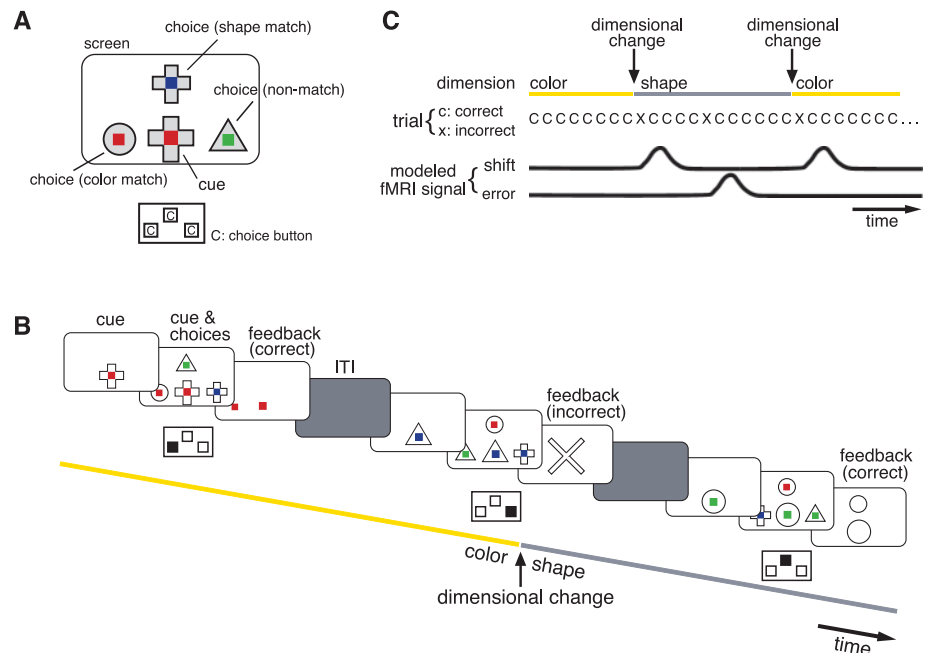


**Fig. 1.** The behavioral task and strategy for event-related fMRI analysis. (A) Visual stimuli. A cue and three choice stimuli were presented on a screen. Among the choice stimuli, one is matched to the cue stimulus in the color dimension, another in the shape dimension, and the other in neither dimension. Subjects were required to match the cue stimulus to one of choice stimuli based on currently relevant dimension by pressing one of the three buttons. (20). (B) Task sequence. In each trial, first a cue stimulus is presented, and then three choice stimuli. Visual feedback notifies subjects whether a response is correct or not. After several successive correct matches, the relevant dimension was changed (dimensional change, arrow). ITI, intertrial interval (19). (C) An event-related fMRI analysis. FMRI signal for each set-shifting event and error trial were modeled independently (25).

<sup>1</sup>Department of Physiology, <sup>2</sup>Department of Neurology, The University of Tokyo School of Medicine, 7-3-1 Hongo, Bunkyo-ku, Tokyo 113-0033, Japan. <sup>3</sup>National Institute for Physiological Sciences, Myodaiji-cho, Okazaki 444-8585, Japan.

\*To whom correspondence should be addressed. E-mail: yasushi\_miyashita@m.u-tokyo.ac.jp

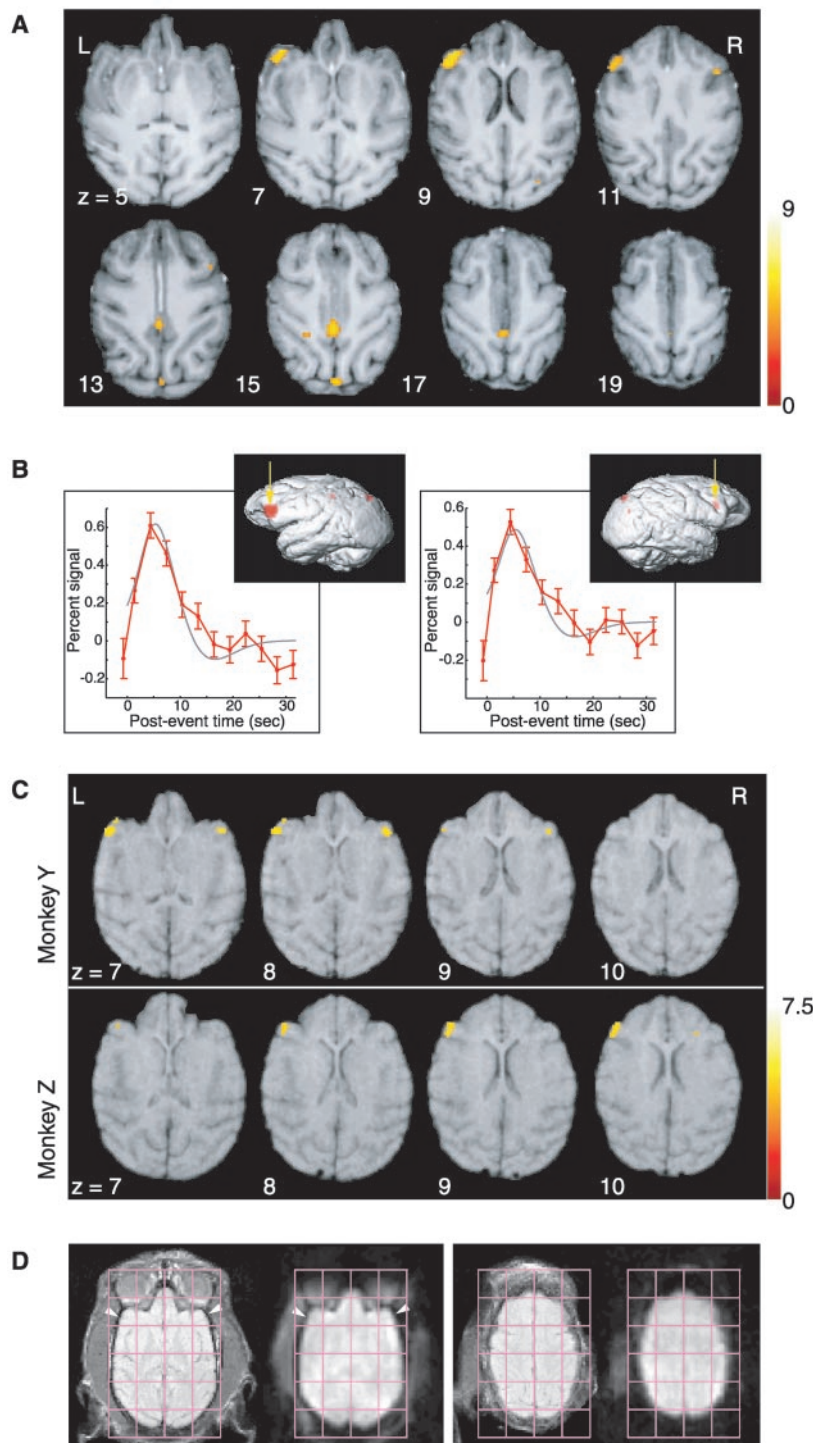


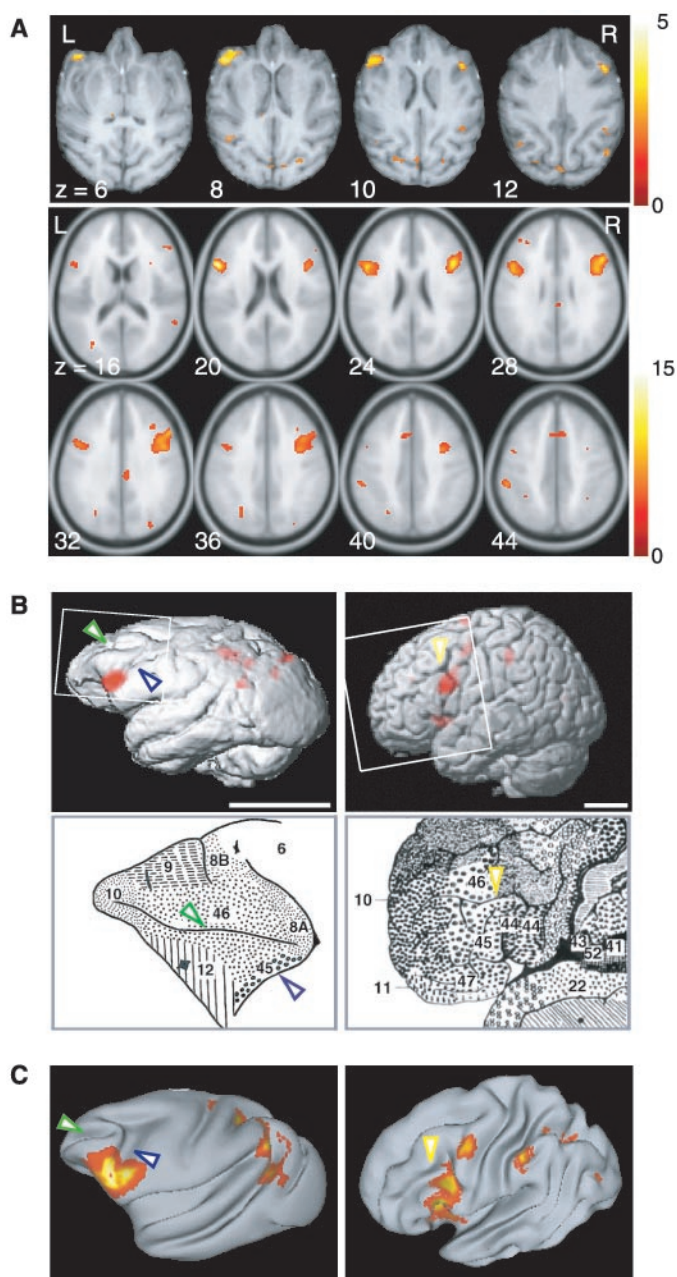
**Fig. 2.** Shift-related activation in monkeys. **(A)** Set-shifting related activation in monkeys revealed by a group analysis. Areas that showed shift-related activation were superimposed on transverse sections of normalized anatomical images. In Fig. 2, A and C, statistical threshold was  $P < 0.05$  corrected for multiple comparisons across the brain volume examined. Color scales indicate  $t$  values. **(B)** Event-related, averaged time courses with the fitted models of hemodynamic response function. The activities are taken from the peak voxels in the left (left panel:  $x = -20, y = 13, z = 9$ ) and the right (right panel:  $x = 18, y = 10, z = 11$ ) inferior prefrontal convexity. Lateral views of 3D-rendering of a monkey brain are presented in insets, and arrows point to activated regions in the inferior prefrontal cortex. **(C)** Intersubject reproducibility of the prefrontal activation. Shift-related activation of each monkey was estimated independently and was superimposed on anatomical images of each monkey. **(D)** Comparison of EPI images (right in each panel) and the corresponding reference images (left in each panel). The slices at the level of the inferior prefrontal cortex and the principle sulcus were shown. Arrowheads indicate the ventral end of the inferior ramus of the arcuate sulcus. Individual grid elements are 14 mm square.

ulation from a relatively small number of subjects (27). The resultant activations were reproducibly found in the rostral bank of the arcuate sulcus or the caudalmost part of the inferior prefrontal convexity, the left intraparietal sulcus, the posterior cingulate, and the precuneus (Fig. 3A, upper).

We further proceeded to fMRI sessions with human subjects using the same task sequence and visual stimuli as in the monkey experiments (28). Functional images from 10 human participants were subjected to an event-related analysis as in the monkey experiments (25), and a random effect model was used to estimate the data ( $P < 0.001$ , uncorrected; 19 or more contiguous voxels) (29). The most prominent shift-related activation of the PFC was found in the posterior part of the bilateral inferior frontal sulcus (Fig. 3A, lower) (26). This focus conforms to the one reported in our previous studies of set shifting [see table 2 in (29)]. This activation was presumably related to the inhibition of the previously relevant response (9). Activated regions were also found in the extrastriate cortex, the inferior parietal lobule, and the anterior insula (26). In the present task condition the parietal activation was weaker than that observed in the previous studies; nevertheless, the global activation pattern including the main activation focus in the PFC was consistent with the preceding studies (29–33).

These fMRI experiments enabled us to compare directly the functional organization of the PFC in monkeys and humans. In the monkeys, the two types of group analysis consistently revealed prominent activation foci at the ventral end of the inferior ramus of the arcuate sulcus or caudalmost part of the inferior convexity [Figs. 2, A and B, and 3A (upper)]. On the other hand, in the humans, prominent activation foci were found in the posterior part of the inferior frontal sulcus (Fig. 3A, lower). Thus the main shift-related activation was commonly found in the posterior part of the ventrolateral PFC across the two species. We hypothesize that these activated regions in the PFC could be functionally homologous regions across the two species with regard to cognitive set-shifting function (Fig. 3, B and C). Estimated cortical areas of these regions corresponded to area 45/posterior12 by Walker (34) or area 45B/45A/44 by Petrides and Pandya (3) in monkeys and Brodmann's area (BA) 44/45 in humans (35) (Fig. 3B). Thus, in our set-shifting paradigm, the functionally homologous regions are largely equivalent in cytoarchitecture across the two species. However, this consistency is not always the case. The frontal eye field, a major region responsible for control of the saccadic eye-movement in the frontal cortex, is assigned to BA 8 in monkeys by electrophysiological and micro-

**Fig. 3.** Comparisons of shift-related activation in the PFC between monkeys and humans. (A) (upper) Shift-related activation in monkeys estimated by a conjunction analysis. A threshold of  $P < 0.001$  (uncorrected) was used for display purpose. (lower) Shift-related activation in humans estimated by a random-effect model ( $P < 0.001$ , uncorrected). (B) Lateral views of 3D-rendered brain image on which the activation shown in (A) was superimposed (upper left, monkeys; upper right, humans). In the human data, prominent activation focus in the posterior part of the inferior frontal sulcus was shown. Other activations in the precentral gyrus and in the anterior insula were also observed. For references, cytoarchitectonic map of macaque monkeys by Walker (lower left) (34) and that of humans by Brodmann (lower right) (35) were presented. These maps correspond approximately to areas in the white squares in the upper panels. Green arrowhead, the principal sulcus; blue arrowhead, the inferior ramus of the arcuate sulcus; yellow arrowhead, the inferior frontal sulcus. Scale bar, ~30 mm. (C) The same activation as in (B) were displayed on an inflated surface reconstruction of a monkey brain (left) and that of a human brain (right) (12, 39). Symbols are denoted as in (B).



stimulation studies (36), whereas it is assigned to BA 6 in humans by neuroimaging studies (37). This diversity emphasizes the importance of direct functional comparison of the PFC between species.

**References and Notes**

1. J. M. Fuster, *The Prefrontal Cortex: Anatomy, Physiology, and Neuropsychology of the Frontal Lobe* (Lippincott, Williams & Wilkins, Philadelphia, ed. 3, 1997).
2. P. S. Goldman-Rakic, in *Handbook of Physiology*, section 1, *The Nervous System*, vol. 5, parts 1 and 2, *Higher Functions of the Brain*, F. Plum, Ed. (American Physiological Society, Bethesda, 1987), pp. 373–417.
3. M. Petrides, D. N. Pandya, in *Handbook of Neuropsychology*, vol. 9, F. Boller, J. Grafman, Eds. (Elsevier, Amsterdam, 1994), pp. 17–58.
4. R. E. Passingham, *Neuropsychologia* **10**, 41 (1972).

5. R. Dias, T. W. Robbins, A. C. Roberts, *Nature* **380**, 69 (1996).
6. H. Damasio, A. R. Damasio, *Lesion Analysis in Neuropsychology* (Oxford Univ. Press, New York, 1989).
7. E. K. Miller, J. D. Cohen, *Annu. Rev. Neurosci.* **24**, 167 (2001).
8. B. Milner, *Arch. Neurol.* **9**, 100 (1963).
9. A. M. Owen et al., *Brain* **116**, 1159 (1993).
10. L. G. Ungerleider, S. M. Courtney, J. V. Haxby, *Proc. Natl. Acad. Sci. U.S.A.* **95**, 883 (1998).
11. Y. Miyashita, T. Hayashi, *Curr. Opin. Neurobiol.* **10**, 187 (2000).
12. D. C. Van Essen et al., *Vision Res.* **41**, 1359 (2001).
13. L. Stefanacci et al., *Neuron* **20**, 1051 (1998).
14. D. J. Dubowitz et al., *Neuroreport* **9**, 2213 (1998).
15. N. K. Logothetis, H. Guggenberger, S. Peled, J. Pauls, *Nature Neurosci.* **2**, 555 (1999).
16. T. Hayashi, S. Konishi, I. Hasegawa, Y. Miyashita, *Eur. J. Neurosci.* **11**, 4451 (1999).
17. G. A. Orban, *Curr. Opin. Neurobiol.* **14**, 47 (2001).
18. W. Vanduffel et al., *Neuron* **32**, 565 (2001).

19. At the start of each trial, a cue stimulus was presented on a screen for 500 ms. Three choice stimuli were then presented at the top, left, and right of the cue stimulus. Each stimulus consisted of a color patch (red, blue, or green) superimposed on a gray shape (circle, triangle, or cross); therefore, each stimulus has two stimulus dimensions: color and shape. Among the three choice stimuli, one was matched to the cue stimulus in the color dimension, one was matched in the shape dimension, and the other stimulus was not matched in either dimension (Fig. 1A). Only one dimension was considered relevant in determining the correct match at a given time during the task, and subjects were required to respond to one of the three choice stimuli by matching the attribute of the central cue stimulus according to the present relevant dimension. After six to eight successive correct trials, the currently relevant dimension was changed to the other dimension without any notice (dimensional change). To resume making correct matches after these dimensional changes, subjects had to shift their cognitive set based on the feedback stimuli so that they adapted to the other dimension (therefore, there was no major contribution of working memory here) (Fig. 1B).

20. Visual stimuli were projected from an LCD projector onto a screen. Optic fiber-based, MR-compatible buttons were used for subjects' responses. Subjects responded by pressing one of three buttons corresponding to a choice stimulus (Fig. 1, A and B). They were notified via visual feedback as to whether their response was correct or not. In the case of a correct choice, only the matched shapes or color patches remained on the screen as a "correct" visual feedback for 1 s. For monkey subjects, a liquid reward was delivered at the onset of the feedback. In the case of an incorrect response, an "X" was presented to both monkey and human subjects as an "incorrect" feedback for 1 s, and no reward was delivered to monkey subjects. Intertrial intervals were 2 s. To see the effect of eye movements, we conducted separate behavioral experiments in which we recorded eye movements in monkey and human subjects while they performed the task (38). We compared saccade frequencies during set shifting and after the completion of set shifting, and found no significant difference between these two periods in humans (during set shifting  $1.4 \pm 0.6$ ; after completion of set shifting  $1.3 \pm 0.6$ ; mean  $\pm$  SD,  $n = 40$ ,  $P > 0.34$ , paired  $t$  test) and in monkeys (during set shifting  $2.4 \pm 0.8$ ; after completion of set shifting  $2.5 \pm 0.9$ ;  $n = 40$ ,  $P > 0.45$ ). From these behavioral results, together with the fact that the locations of the activation peak were distinct from the center of the frontal eye-field in both humans and monkeys (26, 36, 37), it is unlikely that the observed activation was related to the eye movements.

21. Animal experiments were conducted in accordance with the NIH guidelines for the care and use of laboratory animals and the regulations of the University of Tokyo School of Medicine. We used two monkeys (*Macaca fuscata*). Before MR scanning, plastic MR-compatible head-holders were implanted in the monkeys under general anesthesia with sodium pentobarbital under aseptic conditions. After recovery, the monkeys were adapted to the posture and the noise during scanning. All of these adaptations were conducted in a laboratory room without using a mock-up of the MR bore.

22. The time of completion of set shifting was defined as the beginning of three or more consecutive correct trials after the dimensional changes.

23. Functional imaging of monkeys was performed on a 1.5 T scanner (Hitachi Medical Corp., Tokyo) with a horizontal bore (inner diameter of 540 mm). A quadrature coil (inner diameter of 190 mm) was used as a radio-frequency (RF) probe. During the imaging sessions, the monkey's head was fixed with the head-holders to make the relative head position to the scanner constant. To minimize licking movements during reward delivery, a mouthpiece was used in the monkey experiments. We found no considerable change of image quality by the licking movements and no additional movement of the monkeys in case of incorrect responses. Four-segmented gradient-

echo echo-planar imaging (GE-EPI) was used; field of view (FOV) = 128 × 128 mm, repetition time (TR) = 750 ms, echo time (TE) = 18.4 or 20 ms, flip angle = 64 degrees, matrix = 64 × 64, slice thickness = 2 mm, interslice gap = 0.5 mm, 9 transverse slices]. Image distortions from the susceptibility artifact were negligible, and the EPI-images overlapped faithfully with the reference images (Fig. 2D). Functional images were first realigned, spatially normalized to a template with interpolation to a 1 × 1 × 1 mm space and then smoothed with a Gaussian kernel [full width at half maximum (FWHM) 4 mm]. The template was made from 3D-structural images of one monkey's whole brain (24) and was arranged in bicommissural space (16). The origin was placed at the anterior commissure. In separate sessions, high-resolution 3D-anatomical scans of monkeys were obtained using both the 3D-gradient-echo sequence (voxel = 1 × 1 × 1 mm) and the 3D-MDEFT (modified driven equilibrium Fourier transform) sequence (voxel = 0.5 × 0.5 × 0.5 mm).

24. J. Ashburner, K. J. Friston, *NeuroImage* **6**, 209 (1997).  
 25. Data were analyzed using the general linear model for event-related designs in SPM99 (<http://www.fil.ion.ucl.ac.uk/spm/>). Transient events during dimensional changes were coded using the hemodynamic response function implemented in SPM 99. The onset of each hemodynamic response function was aligned at the

onsets of the incorrect feedback stimuli just before the completion of each shifting (Fig. 1C). Error trials were coded independently. In monkey experiments, statistical results are based on a single-voxel threshold of  $P < 0.05$ , corrected for multiple comparisons across the brain volume examined. In human experiments, a random effect model was used for estimating the data, and we assessed statistical significance at the threshold of 19 or more contiguous significant voxels above the  $P < 0.001$  (uncorrected) (29).

26. Supplementary materials of Tables 1 and 2 are available on Science Online at [www.sciencemag.org/cgi/content/full/295/5559/1532/DC1](http://www.sciencemag.org/cgi/content/full/295/5559/1532/DC1)  
 27. K. J. Friston, A. P. Holmes, K. J. Worsley, *NeuroImage* **10**, 1 (1999).  
 28. In human experiments, informed consent was obtained from ten healthy right-handed subjects. They were scanned using experimental procedures approved by the institutional review board of the University of Tokyo School of Medicine. Functional MRI scans were performed on the same 1.5 T scanner as in the monkey experiments with single-shot GE-EPI (FOV = 256 × 256 mm, TR = 4 s, TE = 50 ms, flip angle = 90 degrees, matrix = 64 × 64, slice thickness = 4 mm, 28 transverse slices). Functional images were realigned, spatially normalized to a template with interpolation to a 2 × 2 × 2 mm space, and smoothed with a Gaussian kernel (FWHM 8 mm).

29. S. Konishi, D. I. Donaldson, R. L. Buckner, *NeuroImage* **13**, 364 (2001).  
 30. K. F. Berman *et al.*, *Neuropsychologia* **33**, 1027 (1995).  
 31. Y. Nagahama *et al.*, *Brain* **119**, 1667 (1996).  
 32. S. Konishi *et al.*, *Nature Neurosci.* **1**, 80 (1998).  
 33. O. Monchi, M. Petrides, V. Petre, K. Worsley, A. Dagher, *J. Neurosci.* **21**, 7733 (2001).  
 34. A. E. Walker, *J. Comp. Neurol.* **73**, 59 (1940).  
 35. K. Brodmann, in *Handbuch der Neurologie*, M. Lewandowsky, Ed. (Springer-Verlag, Berlin, 1910), vol. 1, pp. 206–307.  
 36. C. J. Bruce, M. E. Goldberg, M. C. Bushnell, G. B. Stanton, *J. Neurophysiol.* **54**, 714 (1985).  
 37. T. Paus, *Neuropsychologia* **34**, 475 (1996).  
 38. I. Hasegawa, T. Fukushima, T. Ihara, Y. Miyashita, *Science* **281**, 814 (1998).  
 39. Surface-based activation displays were constructed using the SureFit software (<http://stp.wustl.edu/>) (12).  
 40. We thank I. Hasegawa, M. Morita, M. Koyama, and M. Ohbayashi for their help and I. Kanazawa for his encouragement. This work was supported by a Grant-in-Aid for Specially Promoted Research (07102006) from the Ministry of Education, Culture, Sports, Science and Technology (MEXT) of Japan.

1 November 2001; accepted 15 January 2002

# Retrograde Support of Neuronal Survival Without Retrograde Transport of Nerve Growth Factor

Bronwyn L. MacLinnis and Robert B. Campenot\*

Application of nerve growth factor (NGF) covalently cross-linked to beads increased the phosphorylation of TrkA and Akt, but not of mitogen-activated protein kinase, in cultured rat sympathetic neurons. NGF beads or iodine-125-labeled NGF beads supplied to distal axons resulted in the survival of over 80% of the neurons for 30 hours, with little or no retrograde transport of iodine-125-labeled NGF; whereas application of free iodine-125-labeled NGF (0.5 nanograms per milliliter) produced 20-fold more retrograde transport, but only 29% of the neurons survived. Thus, in contrast to widely accepted theory, a neuronal survival signal can reach the cell bodies unaccompanied by the NGF that initiated it.

The literatures of neuronal development, neurotrauma, degenerative neurological disease, and neuronal regeneration are pervaded by the concept that the survival and function of neurons depend on retrograde transport of neurotrophic factors released from the target cells that they innervate. This idea began with the discovery that nerve growth factor (NGF) is retrogradely transported from axon terminals to neuronal cell bodies (1–7). The current theory, that NGF complexed with its receptor, TrkA, is endocytosed, trafficked to signaling endosomes (8, 9), and retrogradely

transported to the cell bodies, has been supported by results of studies with compartmented cultures (10–14). However, Senger and Campenot (15) observed retrograde phosphorylation of TrkA and other proteins occurring 1 to 15 min after NGF application, preceding the arrival of detectable <sup>125</sup>I-NGF by at least 30 min.

We examined this issue using NGF covalently cross-linked to beads to prevent internalization (16). Mass cultures of rat sympathetic neurons (17) that had been deprived of NGF (18) displayed a similar level of phosphorylation of TrkA (19) after 1 hour of application of free NGF (50 ng/ml) or NGF beads (50 μl/ml) (Fig. 1A). NGF and NGF beads also induced the phosphorylation of Akt (Fig. 1B), the latter suggesting that phosphorylated TrkA (pTrkA) at the plasma

membrane can activate phosphatidylinositol 3-kinase (PI 3-kinase). In contrast, little mitogen-activated protein kinase (MAPK) phosphorylation was observed in response to NGF beads (Fig. 1B), suggesting that internalization of pTrkA is necessary for the activation of MAPK. This result is consistent with reports that the blockage of endocytosis of TrkA, by means of pharmacological inhibitors or dominant-negative dynamin, inhibits NGF-induced MAPK phosphorylation in dorsal root ganglion neurons (20) and PC12 cells (20–22). Thus, the lack of NGF-induced MAPK phosphorylation that we observed suggests that neither NGF nor TrkA is internalized when NGF is presented in bead-linked form.

To determine whether NGF beads can produce retrograde signals, distal axons of sympathetic neurons in NGF-deprived compartmented cultures (17, 18) received different NGF treatments for 30 hours, and neuronal survival was assayed (23). Treatment with NGF beads resulted in 81% neuronal survival (Fig. 2, A and B), which approaches the survival in cultures given free NGF (50 ng/ml) (95%) and is almost four times the survival of cultures given no NGF (22%). Control beads to which NGF was not covalently cross-linked did not support survival (Fig. 2B). Retrograde survival could conceivably have been achieved by the release of NGF from the beads into the culture medium, followed by internalization and retrograde transport. However, supernatant media from NGF beads that had supported 30 hours of retrograde survival of one set of cultures (Fig. 2C, solid bars) failed to support survival of a second set of cultures (Fig. 2C, hatched bars), whereas free NGF from the first set again supported the survival of a second set. Supernatant media from NGF beads that were preincubated

Department of Cell Biology, 6–14 Medical Sciences Building, University of Alberta, Edmonton, Alberta, Canada, T6G 2H7.

\*To whom correspondence should be addressed. E-mail: bob.campenot@ualberta.ca